EPJ manuscript No.
(will be inserted by the editor)

Nonlinear waves over highly variable topography

André Nachbin[2,a] and Wooyoung Choi[1,b]

[1] IMPA, Rio de Janeiro, RJ, 22460-320, Brazil
[2] Dept. of Math. Sci., New Jersey Institute of Technology, Newark, NJ, 07102-1982, USA

Abstract. This paper reviews the authors' recent work on water waves in heterogeneous media, namely nonlinear reduced models for water waves propagating over a region of highly variable depth. Both surface and internal waves are considered. Through different strategies for the mathematical modeling, at the level of equations, we show how diferent types of water wave models (namely systems of partial differential equations) can arise: weakly or fully dispersive, weakly or strongly nonlinear. The applications for these types of long waves are usually from Geophysics: in particular oceanography and meteorology. Here the emphasis is on coastal waves related to Physical Oceanography. An overview of the mathematical formulation is presented together with different asymptotic simplifications at the level of the partial differential equations (PDEs). References for recent work on the asymptotic analysis of solutions is also provided. These describe the regime where long pulse shaped waves propagate over rapidly varying topographic heterogeneities, which are modeled through rapidly varying coefficients in the PDEs.

1 Introduction

This article reviews the authors' recent work on deducing reduced models for water waves in a highly complex geometry. Both surface and internal waves are considered. These reduced models are then used for analyzing nonlinear waves in complex systems, where the complicated geometry of the two-dimensional problem is converted into one-dimensional systems of partial differential equations (PDEs) with highly variable coefficients.

Waves in heterogeneous media is a field of great mathematical interest and, not surprisingly, applicable to many technological and environmental problems. If we keep our attention to Geophysics we have applications in the atmosphere, hydroshpere and lithosphere. In the lithosphere one may think of acoustic waves, regarding the seismic probing of the Earth's subsurface [1]. This is of interest to the oil industry. In the atmosphere and hydrosphere we may take the heterogeneous medium as being the topography. These physical applications, for long wave interactions with topography, range from coastal surface waves [2] to atmospheric flows over mountain ranges [3, 4].

In this work we will focus on surface and internal coastal waves. Waves on/in an ideal fluid body, under the force of gravity, are governed by the Euler equations. Nevertheless in both engineering applications as well as laboratory scales, the full Euler equations appears more complex than necessary. Very often this system, for the entire fluid body, can be simplified to more tractable reduced surface/internal wave models, when restricted to specific physical regimes. Under this modeling strategy Boussinesq-type equations, which include leading order terms regarding nonlinearity and dispersive effects, have been shown to provide an accurate

[a] e-mail: nachbin@impa.br
[b] e-mail: wychoi@njit.edu

description for wave evolution in coastal regions. The first set of equations valid for variable depth was derived by Peregrine [5] in 1967. The model is valid under the mild slope hypothesis.

Very recently there has been a great amount of research regarding additional modeling issues, namely in improving Boussinesq-type models as for example in [6–9,11,10]. But all of these consider flat or slowly varying topographies. For very general topographies a terrain-following Boussinesq model was developed by Nachbin [12] in 2003. The model allows for multiply-valued topography profiles, as will be shown here. Solutions to this model were analyzed in [13–16]. Existence and uniqueness for a variable coefficient Boussinesq system of equations was first given by Quintero and Muñoz in 2004 [17].

Then ideas from Nwogu [9] were used to generalize the reduced model given in [12]. We showed how small (higher order) changes in the linear dispersion relation (over a flat bottom) become dramatically important in the presence of a highly-fluctuating topography [18]. We presented a linear dispersion analysis and validated the corresponding results both for a flat bottom and also in the presence of a variable propagation medium. In order to fully validate dispersive properties of several possible truncations, that can be made for these Boussinesq-type models, we compared them with the corresponding complete (non-truncated) model, namely linear potential theory. For the numerical validation in [18] we used a new, highly efficient numerical scheme developed by Artiles and Nachbin [19,20]. Discrepancies observed become even more important in the *waveform inversion problem* [21], an application for determining (for example) a *tsunami's initial profile* [18].

For internal gravity waves at the interface between two layers of different densities, various asymptotic models including the Boussinesq-type equations have been proposed and studied mainly under the traditional weakly nonlinear assumption. An increasing number of recent field observations of large amplitude long internal waves, however, indicate that the previously known weakly nonlinear models are no longer applicable to the strongly nonlinear regimes and it is crucial to develop new dynamical models whose range of validity is large enough to describe realistic observations. It has been shown in Choi and Camassa [52,53] that, using a systematic asymptotic expansion, such models can be derived in a two-layer system and their solitary wave solutions agree well with both numerical solutions of the Euler equations and laboratory experiments [55]. In their derivation, the thickness of one of the two layers is assumed to be small compared with the characteristic wavelength, but no assumption on the wave amplitude has been made. In this review, we focus on the strongly nonlinear models for flat bottom and discuss possible extensions to variable bottom.

2 Reduced surface wave models: weak dispersion

2.1 Formulation and background of the problem

In this section we start with the more standard (reduced model) derivation procedure in order to obtain a family of reduced governing equations as studied in many papers indicated later in this work.

When the fluid, where surface waves are propagating, can be considered as being inviscid the Navier-Stokes equations reduce to the Euler equations [2,22]. When the free surface flow can be taken as being incompressible and irrotational it is interesting to recast the Euler equations into a potential theory framework [22]. For example in a two-dimensional flow, we can study the evolution of the velocity potential (one object) as opposed to the evolution of two objects, the horizontal e vertical velocities. As will be seen below, we can also take advantage of many theoretical aspects of harmonic functions as well as the associated complex analysis.

Let variables with physical dimensions be denoted with a tilde. Then the formulation through the velocity potential $\tilde{\phi}$, where $(u, v) \equiv \nabla\tilde{\phi}$ is the velocity vector, is given as

$$\tilde{\phi}_{\tilde{x}\tilde{x}} + \tilde{\phi}_{\tilde{y}\tilde{y}} = 0 \quad \text{for} \quad -\tilde{H}(\tilde{x}) < \tilde{y} < \tilde{\eta}(\tilde{x}, \tilde{t}), \quad -\infty < \tilde{x} < \infty,$$

subject to

$$\tilde{\eta}_{\tilde{t}} + \tilde{\phi}_{\tilde{x}}\tilde{\eta}_{\tilde{x}} - \tilde{\phi}_{\tilde{y}} = 0,$$

$$\tilde{\phi}_{\tilde{t}} + \frac{1}{2}\left(\tilde{\phi}_{\tilde{x}}^2 + \tilde{\phi}_{\tilde{y}}^2\right) + g\tilde{\eta} = 0$$

at the free surface $\tilde{y} = \tilde{\eta}(\tilde{x}, \tilde{t})$. At the impermeable bottom topography we have a Neumann condition.

We introduce the length scales ℓ_p (a typical pulse width or wavelength), h_0 (a typical depth), a_o (a typical wave amplitude), ℓ (the horizontal length scale for bottom irregularities) and L (the total length of the rough region or the total propagation distance). The acceleration due to gravity is denoted by g and the reference shallow water speed is $c_0 = \sqrt{gh_0}$. Dimensionless variables are then defined in a standard fashion [23,22] by having

$$\tilde{x} \;=\; \ell_p\, x \qquad \tilde{y} \;=\; h_0\, y \qquad \tilde{t} \;=\; \left(\frac{\ell_p}{c_0}\right) t$$

$$\tilde{\eta} \;=\; a\, \eta \qquad \tilde{\phi} \;=\; \left(\frac{g\ell_p\, a}{c_0}\right)\phi \qquad \tilde{h} \;=\; h_0\, H\left(\frac{\tilde{x}}{l_b}\right).$$

The dimensionless form of the potential theory formulation for Euler's equations with a free surface and an impermeable bottom topography [22] is

$$\beta\, \phi_{xx} + \;\phi_{yy} \;=\; 0 \quad \text{for} \quad -H(x/\gamma) < y < \alpha\eta(x,t), \qquad -\infty < x < \infty, \tag{1}$$

subject to

$$\eta_t + \alpha\phi_x\eta_x - \frac{1}{\beta}\phi_y = 0, \tag{2}$$

$$\eta + \phi_t + \frac{\alpha}{2}\left(\phi_x^2 + \frac{1}{\beta}\phi_y^2\right) = 0 \tag{3}$$

at the free surface $y = \alpha\eta(x,t)$. The function $\phi(x,y,t)$ denotes the dimensionless velocity potential, $\eta(x,t)$ the dimensionless wave elevation measured with respect to the undisturbed free surface $y = 0$. The dimensionless parameters $\alpha = a_o/h_o$ and $\beta = h_o^2/\ell_p^2$ measure the strength of nonlinear and dispersive effects, respectively, and the parameter $\gamma = \ell/\ell_p$ measures the ratio inhomogeneities/wavelength. We recall that in the potential theory model the fluid is assumed to be inviscid, incompressible and irrotational.

At the impermeable bottom the Neumann condition

$$\phi_y + \frac{\beta}{\gamma}\, H'(x/\gamma)\phi_x = 0 \tag{4}$$

is satisfied. We assume that the boundary at the bottom is described by the function $y = -H(x/\gamma)$ where

$$H(x/\gamma) \;=\; \begin{cases} 1 + n(x/\gamma) & \text{when } \; 0 < x < L \\ 1 & \text{when } \; x \le 0 \;\text{ or }\; x \ge L. \end{cases} \tag{5}$$

The bottom profile is described by the (possibly rapidly varying) function $n(x/\gamma)$. We point out that the topography is rapidly varying when $\gamma \ll 1$. The undisturbed depth is given by $y = -1$ and the topography can be of large amplitude provided that $|n| < 1$. The fluctuations n are not assumed to be small, nor continuous, nor slowly varying.

Our main interest is to order the parameters α, β and γ as powers of ε and analyse the solution in the limit $\varepsilon \downarrow 0$. For example for $\alpha = \beta = O(\varepsilon) \ll 1$ we may consider solitary waves. Moreover when also $\gamma = O(\varepsilon)$ we have long waves interacting with rapidly varying heterogeneities, in this case the topography. The problem in its present form is extremely complicated. Hence simplifying the mathematical model (namely the PDE) is of interest in

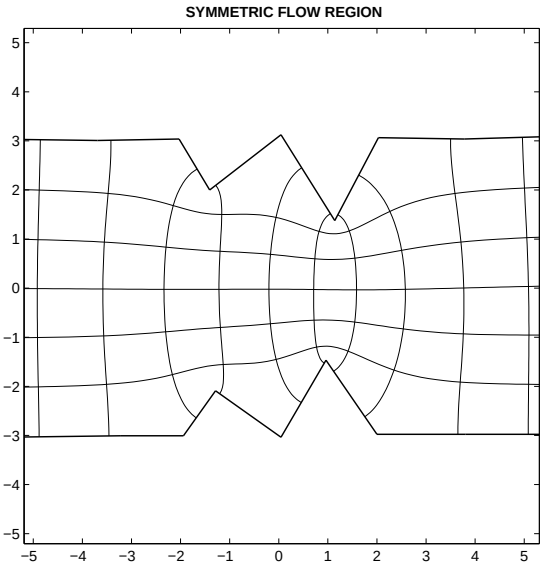

Fig. 1. The symmetric domain in the complex z-plane, where $z = x(\xi, \tilde{\zeta}) + i\tilde{y}(\xi, \tilde{\zeta})$. The lower half ($x \in [-5, 5]$, $y \in [-3, 0]$) is the physical channel with $y = \tilde{\zeta} = 0$ indicating the undisturbed free surface. Superimposed in this complex z-plane domain are the (curvilinear) coordinate level curves from the w-plane system $\xi\tilde{\zeta}$. The polygonal line at the bottom of the figure is a schematic representation of the topography (where $\tilde{\zeta} = \pm\sqrt{\beta}$). This figure was generated using SC-Toolbox [24,25].

order to perform an asymptotic ($\varepsilon \to 0$) analysis. A key issue is not to oversimplify the model and eliminate phenomena of physical and mathematical interest.

Thus in order to simplify the geometry of the problem and enable the asymptotic analysis of equations (1)-(5), we define a symmetric flow domain by reflecting the original one about the undisturbed free surface. In this symmetric domain (figure 1) we use curvilinear coordinates defined through the conformal mapping of this region. This strategy was already employed in [35] and [12]. For completeness we summarize the main ingredients of the asymptotic analysis in curvilinear coordinates. The symmetric domain is denoted by Ω_z where $z = x + i\sqrt{\beta}y$ and it can be considered as the conformal image of the strip Ω_w where $w = \xi + i\tilde{\zeta}$ with $|\tilde{\zeta}| \leq \sqrt{\beta}$. Note that the topography is defined along the curve $\tilde{\zeta} \equiv -\sqrt{\beta}$. Then $z = x(\xi, \tilde{\zeta}) + i\ \sqrt{\beta}y(\xi, \tilde{\zeta}) = x(\xi, \tilde{\zeta}) + i\ \tilde{y}(\xi, \tilde{\zeta})$ where x and $\tilde{y}$ are a pair of harmonic functions on Ω_w. In figure 2, we present a scheme which explains the changes of variables to be introduced in the sequel.

The scaled water wave equations in the fixed orthogonal curvilinear coordinates $(\xi, \tilde{\zeta})$ are:

$$\phi_{\xi\xi} \ + \ \phi_{\tilde{\zeta}\tilde{\zeta}} \ = \ 0, \qquad -\sqrt{\beta} < \tilde{\zeta} < \alpha\sqrt{\beta}N(\xi, t), \tag{6}$$

with free surface conditions

$$|J|N_t + \alpha\phi_\xi N_\xi - \frac{1}{\sqrt{\beta}}\phi_{\tilde{\zeta}} = 0 \tag{7}$$

and

$$\phi_t + \eta + \frac{\alpha}{2|J|}\left(\phi_\xi^2 + \phi_{\tilde{\zeta}}^2\right) = 0 \tag{8}$$

at $\tilde{\zeta} = \alpha\sqrt{\beta}N(\xi, t)$. The bottom boundary condition (4) transforms into the trivial condition

$$\phi_{\tilde{\zeta}} = 0 \qquad \text{at} \ \ \tilde{\zeta} = -\sqrt{\beta}. \tag{9}$$

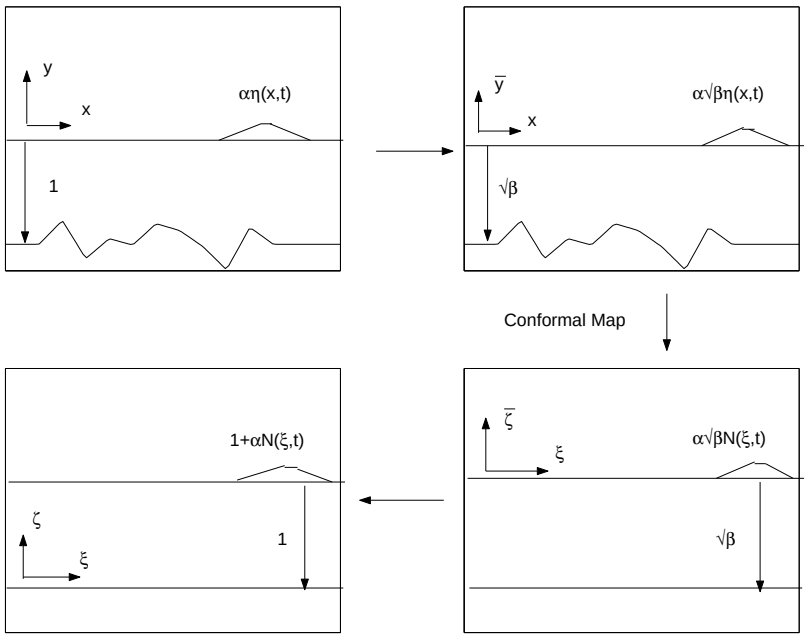

Fig. 2. Schematic plot which explains the changes of variables introduced in the derivation of the extended Boussinesq equations. The conformal map transforming the rectangular coordinates $(x, \tilde{y})$ onto the curvilinear coordinates $(\xi, \tilde{\zeta})$ is indicated in this plot.

The function $N(\xi, t)$ denotes the position of the free surface in the new coordinate system and $|J|$ denotes the Jacobian of the change of coordinates:

$$|J| = x_\xi \tilde{y}_{\tilde{\zeta}} - \tilde{y}_\xi x_{\tilde{\zeta}} = \tilde{y}_{\tilde{\zeta}}^2 + \tilde{y}_\xi^2.$$

At this point, it is convenient to let the origin of the curvilinear coordinate system be at the bottom and define $\tilde{\zeta} = \sqrt{\beta}(\zeta - 1)$. See the last picture in the scaling sequence given in figure 2. In the system of coordinates (ξ, ζ), equations (6)-(9) transform into

$$\beta\phi_{\xi\xi} \ + \ \phi_{\zeta\zeta} \ = \ 0, \qquad \text{at} \ \ 0 < \zeta < 1 + \alpha N(\xi, t), \tag{10}$$

with free surface conditions

$$|J| N_t + \alpha\phi_\xi N_\xi - \frac{1}{\beta}\phi_\zeta = 0, \tag{11}$$

$$\eta + \phi_t + \frac{\alpha}{2|J|}\left(\phi_\xi^2 + \frac{1}{\beta}\phi_\zeta^2\right) = 0 \tag{12}$$

at $\zeta = 1 + \alpha N(\xi, t)$ and

$$\phi_\zeta = 0 \qquad \text{at} \ \ \zeta = 0. \tag{13}$$

As in Whitham [22], consider a power series expansion near the bottom of the channel in the form

$$\phi(\xi, \zeta, t) = \sum_{n=0}^{\infty} \zeta^n \ f_n(\xi, t). \tag{14}$$

Asymptotic analysis will be performed at the level of the equations in terms of the small parameters α and β.

By substituting this expression in the scaled Laplace equation (10) and using the Neumann condition (13) at the bottom we can express the potential as a power expansion in β

$$\phi(\xi,\zeta,t) = \sum_{n=0}^{\infty} \frac{(-\beta)^n}{(2n)!}\zeta^{2n}\frac{\partial^{2n} f(\xi,t)}{\partial \xi^{2n}} \tag{15}$$

where, for simplicity, $f(\xi,t) = f_0(\xi,t)$.

Now using that at the smooth free surface $\tilde{\zeta}_{FS} = \alpha\sqrt{\beta}N(\xi,t)$ the Jacobian is

$$|J|(\xi,t) = \tilde{y}^2_{\xi}(\xi,\tilde{\zeta}_{FS}) + \tilde{y}^2_{\tilde{\zeta}}(\xi,\tilde{\zeta}_{FS}),$$

and the Taylor polynomial formula leads to

$$|J|(\xi,t) = \tilde{y}^2_{\tilde{\zeta}}(\xi,0) + \alpha^2 R_J(\xi,\tilde{\zeta}_M) = M(\xi)^2 + O(\alpha^2), \quad 0 < |\tilde{\zeta}_M| < |\tilde{\zeta}_{FS}|. \tag{16}$$

The metric term $M(\xi)$ is defined below. Thus, the Jacobian can be well approximated by an $O(1)$ time independent coefficient. For the same reason, approximating $\tilde{\zeta}(x,\tilde{y}_{FS})$ in $\tilde{y}$ leads to

$$N(\xi,t) = \frac{1}{M(\xi)}\eta(x(\xi),t) + \alpha^2\beta R_N(\xi,\tilde{y}_M), \quad 0 < |\tilde{y}_M| < |\tilde{y}_{FS}|, \tag{17}$$

and we establish a relation between the free surface representation in curvilinear coordinates ($N(\xi,t)$) and in cartesian coordinates ($\eta(x,t)$).

At the undisturbed level we define the **variable free surface coefficient** [12]

$$M(\xi) \equiv \tilde{y}_{\tilde{\zeta}}(\xi,0) = 1 + m(\xi)$$

where

$$m(\xi;\sqrt{\beta},\gamma) \equiv \frac{\pi}{4\sqrt{\beta}} \int_{-\infty}^{\infty} \frac{n(x(\xi_0,-\sqrt{\beta})/\gamma)}{cosh^2\frac{\pi}{2\sqrt{\beta}}(\xi_0-\xi)}d\xi_0 \;=\; (K*(n\circ x))(\xi). \tag{18}$$

The metric term $M(\xi)$ is the leading order term of the Jacobian and is smooth even when the function describing the bottom is discontinuous or non differentiable. Moreover it is time independent and becomes identically one in the case of a constant depth. These features are important when implementing a numerical solver for the Boussinesq formulation.

Introducing the approximations (16), (17) in the equations (10)-(13), it gives

$$\beta\phi_{\xi\xi} \;+\; \phi_{\zeta\zeta} \;=\; 0, \qquad \text{at} \;\; 0 < \zeta < 1 + \alpha\frac{\eta(\xi,t)}{M}, \tag{19}$$

with free surface conditions

$$M\eta_t + \alpha\phi_{\xi}\left(\frac{\eta}{M}\right)_{\xi} - \frac{1}{\beta}\phi_{\zeta} = 0, \tag{20}$$

$$\eta + \phi_t + \frac{\alpha}{2M^2}\left(\phi^2_{\xi} + \frac{1}{\beta}\phi^2_{\zeta}\right) = 0 \tag{21}$$

at $\zeta = 1 + \alpha(\eta(\xi,t)/M(\xi)$ and

$$\phi_{\zeta} = 0 \qquad \text{at} \;\; \zeta = 0. \tag{22}$$

Using the power series expansion for the potential the free surface conditions (20)-(21) can be further approximated as

$$\eta + f_t - \frac{\beta}{2}f_{\xi\xi t} + \frac{\alpha}{2M^2(\xi)}f^2_{\xi} = O(\alpha\beta,\beta^2), \tag{23}$$

$$M(\xi)\ \eta_t + \left[\left(1+\frac{\alpha}{M(\xi)}\eta\right) f_\xi\right]_\xi - \frac{\beta}{6} f_{\xi\xi\xi\xi} = O(\alpha^2, \alpha\beta, \beta^2). \tag{24}$$

The variable coefficients in the system above are time independent and depend only on $\tilde{y}_{\tilde{\zeta}}(\xi, 0)$.

In [12] it is shown that equations (23)-(24) lead to the **terrain-following system**

$$M(\xi)\eta_t + \left[\left(1+\frac{\alpha\ \eta}{M(\xi)}\right) U_o\right]_\xi = 0, \tag{25}$$

$$U_{o,t} + \eta_\xi + \alpha\left(\frac{U_o^2}{2M^2(\xi)}\right)_\xi - \frac{\beta}{3} U_{o,\xi\xi t} = 0, \tag{26}$$

where U_o is the depth averaged velocity

$$U_o(\xi, t) = \frac{1}{\zeta_{FS}} \int_0^{\zeta_{FS}} \phi_\xi(\xi, \zeta, t) d\zeta. \tag{27}$$

As pointed out in Nachbin [12] these are weighted averages along ($\xi \equiv$constant)-curves connecting the undisturbed free surface to the topography (c.f. figure 3). It turns out that the conformal mapping gives more weight near the free surface, than to the regions in the deep valleys, where the topography is rapidly varying. The fact that the ($\zeta = constant$) level curves accumulate more near the free surface has a very positive impact. As mentioned above, physically this means that more emphasis is given to the flow field near the free surface, exactly where the physical model is more accurate. Another very interesting fact is that the curvilinear coordinates preconditions the system of PDEs leading to an underlying eigenvalue representation more amenable for computer simulations [14].

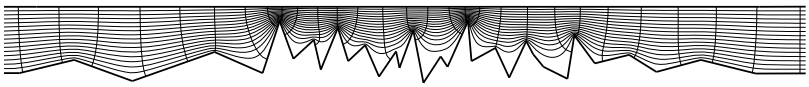

Fig. 3. Multiscale topography with the $\xi - \zeta$ curvilinear coordinate system.

2.2 Asymptotics for pulse shaped solutions

The main objective of the present review is to describe asymptotic strategies in deriving reduced models, namely in doing asymptotics with the partial differential operators. Nevertheless it is important to point out that many papers followed from the new model generated. Namely asymptotic analysis for pulse shaped solutions in the hyperbolic, weakly dispersive and weakly nonlinear regime. In all cases two very interesting phenomena were investigated: the *apparent diffusion* due to the interaction of the surface wave with the topography's disordered microscale as well as the *time reversal refocusing* for waveform inversion of pulse shaped waves. Both deterministic and probabilistic analysis were considered. A comprehensive set of references on this theme can be found in [26–33] and the references within.

2.3 Improved Boussinesq systems

Now instead of using the depth averaged velocity, we will express the evolution equations in terms of the fluid velocity measured at **an intermediate depth**, say at $\zeta = Z_0(\xi)$, with $u(\xi, t) = \phi_\xi(\xi, Z_0(\xi), t)$, where $0 < Z_0(\xi) < 1$. This idea was already applied by Nwogu [9] to

obtain a formally equivalent Boussinesq approximation, in the case where the depth is slow-varying. The purpose was to improve the dispersive characteristics of the resulting reduced model.

Differentiating equation (15) with respect to ξ and evaluating at $\zeta = Z_0(\xi)$, we find that to leading order

$$u(\xi,t) = \phi_\xi(\xi, Z_0, t) = f_\xi - \frac{\beta}{2} Z_0^2 f_{\xi\xi\xi} + O(\beta^2) = \tilde{u} - \frac{\beta}{2} Z_0^2 \tilde{u}_{\xi\xi} + O(\beta^2), \tag{28}$$

where for simplicity, we let $\tilde{u} = \tilde{u}(\xi,t) = f_\xi(\xi,t)$ be the "slip velocity" along the bottom of the channel. As a consequence,

$$\tilde{u} = u(\xi,t) + \frac{\beta}{2} Z_0^2 \tilde{u}_{\xi\xi} + O(\beta^2). \tag{29}$$

Substituting the expression for $\tilde{u}$ (given by the equation above) into equations (23)-(24) and retaining only terms up to $O(\alpha)$, $O(\beta)$, we arrive at the system

$$M(\xi)\eta_t + \left[\left(1 + \frac{\alpha\,\eta}{M(\xi)}\right) u\right]_\xi + \frac{\beta}{2}\left[\left(Z_0^2 - \frac{1}{3}\right) u_{\xi\xi}\right]_\xi = 0, \tag{30}$$

$$u_t + \eta_\xi + \alpha\left(\frac{u^2}{2M^2(\xi)}\right)_\xi + \frac{\beta}{2}(Z_0^2 - 1) u_{\xi\xi t} = 0. \tag{31}$$

An interesting observation is that the system above reduces to the terrain-following system (25)-(26) when we set $Z_0 = \sqrt{1/3}$.

Of particular interest, by letting $Z_0 = \sqrt{2/3}$, and by using $u_\xi(\xi,t) = -M(\xi)\eta_t + O(\alpha,\beta)$, one obtains the model

$$(M(\xi)\eta)_t + \left[\left(1 + \frac{\alpha\,\eta}{M(\xi)}\right) u\right]_\xi - \frac{\beta}{6}(M(\xi)\eta)_{t\xi\xi} = 0, \tag{32}$$

$$u_t + \eta_\xi + \alpha\left(\frac{u^2}{2M^2(\xi)}\right)_\xi - \frac{\beta}{6} u_{\xi\xi t} = 0. \tag{33}$$

System (32)-(33) was presented by Quintero and Muñoz in [17]. The main property of this particular Boussinesq formulation is the existence of a conserved energy-type functional which enables the use of classical tools to demonstrate the global existence of its solutions [17]. We remark that the existence of this conserved quantity is unclear for the Boussinesq model (25)-(26). Of equal importance is the presence of symmetric dispersive terms in both equations of the system (32)-(33), expressed through the operator $\partial_t - \beta/6\partial_{\xi\xi t}$. This operator can be inverted [17] and the system cast into an integro-differential form, so that the fixed point principle can be applied in order to establish local existence of solutions.

Note that the dispersive terms of the model above are modified when we change the level at which the fluid velocity u is measured, i.e. the parameter Z_0. We remark that this degree of freedom (to select the parameter Z_0) allows us to match the linear dispersion relation, corresponding to the Boussinesq approximation (30)-(31), with that of the original potential theory equation (19)-(22) up to a higher order. This will be explained in section 2.4.

Furthermore, recall that all variable coefficients in the model are smooth even when the physical topography profile is described by a discontinuous or even a multi-valued function. We point out that Nwogu [9] obtained a set of equations with dispersive terms similar to those in system (30)-(31) However, the applicability of Nwogu's formulation is restricted to slowly-varying bottom profiles, which is a common feature of other Boussinesq-type formulations, as for instance [5,7,8,11,34,6]. The reason is that in cartesian coordinates the neglected terms of order $O(\alpha^2, \alpha\beta, \beta^2)$ in the Boussinesq model turn out to be large when the detailed features of the topography are small compared to the typical wavelength [35].

In contrast, in the present Boussinesq formulation (30)-(31), the neglected terms of order $O(\alpha^2, \alpha\beta, \beta^2)$ remain small **even when the topography is rapidly varying**. This is due to the use of terrain-following (curvilinear) coordinates [12]. Thus, we expect that the solutions of equations (19)-(22) and system (30)-(31) coincide with good accuracy even when dispersion is significant. When the bottom is described by a complicated function numerical experiments, shown in [14], provide strong evidence on this regard within the range $0 < \beta < 0.05$, $\alpha = 0.001$.

2.4 Linear dispersive properties

To perform an analysis regarding the dispersive terms in equations (30)-(31) it is sufficient to consider the intermediate depth Z_0 to be a constant.

It is important to remark what is expected from the asymptotically simplified Boussinesq model (30)-(31). It would be desirable that its solution approximates, in some sense, the solution of the original potential theory equations (19)-(22), provided that $0 < \alpha \ll 1$, $0 < \beta \ll 1$. Within this regime the high-order terms $O(\alpha^2, \alpha\beta, \beta^2)$ are expected to be negligible with respect to the first order terms retained in the Boussinesq model (30)-(31).

The analytical, dispersion relation, consistency between the Boussinesq system (30)-(31) and the potential formulation of the Euler equations (19)-(22) is a necessary condition so that the new model is able to capture the same (long wave) physical phenomena as the original fluid equations.

To start, consider the linear dispersion relation which leads to the phase velocity

$$C^2 = \frac{\omega^2}{k^2} = \frac{1 - (\beta/2)(Z_0^2 - \frac{1}{3})k^2}{1 - (\beta/2)(Z_0^2 - 1)k^2} \tag{34}$$

for model (30)-(31). Also we have the (full model's) phase velocity for Airy waves given by

$$\begin{aligned} C^2_{\text{Airy}} = \frac{\omega^2}{k^2} &= \frac{1}{\sqrt{\beta}k} tanh(\sqrt{\beta}k) \\ &\approx 1 - \frac{1}{3}(\sqrt{\beta}k)^2 + \frac{2}{15}(\sqrt{\beta}k)^4 - \frac{17}{315}(\sqrt{\beta}k)^6 + O((\sqrt{\beta}k)^8), \end{aligned} \tag{35}$$

corresponding to equations (19)-(22). As mentioned above, the interesting point here is that we can use this degree of freedom (by selecting the parameter Z_0) in order to match the Taylor series expansion of the dispersion relation (35) up to terms of $O((\sqrt{\beta}k)^4)$.

Over several possibilities, however, we can obtain an optimal value of the depth parameter Z_0, by minimizing the relative error of the phase velocity for instance, over the waveband interval $0 < \sqrt{\beta}k < 5$. The result of this process is the value $Z_0 = 0.469$ [9]. It gives a maximum error of 6% for the entire range. In contrast, for the terrain-following system (25)-(26), we obtain a maximum relative error in the same interval of 15%. This is shown in figure 4 where we compare the dispersion relations for the terrain-following system (25)-(26), with the one for formulation (30)-(31) having either $Z_0 = \sqrt{1/5}$ or $Z_0 = 0.469$. The relative error is computed with respect to the linear potential equations (19)-(22). Several numerical experiments were performed in [14] validating this dispersion analysis. It is worth noting that the simulations were done in the presence of highly variable topographies.

3 Fully dispersive surface wave model

Now we will take a further step in our modeling, in such a way that we will not need to truncate the dispersion relation. In a recent paper Matsuno [10] derived a Boussinesq-type model that arises from an expansion in a steepness parameter and not in the dispersion parameter corresponding to a long wave regime as done above. Matsuno develops a method based on the theory of complex functions and a systematic perturbation theory with respect to the steepness

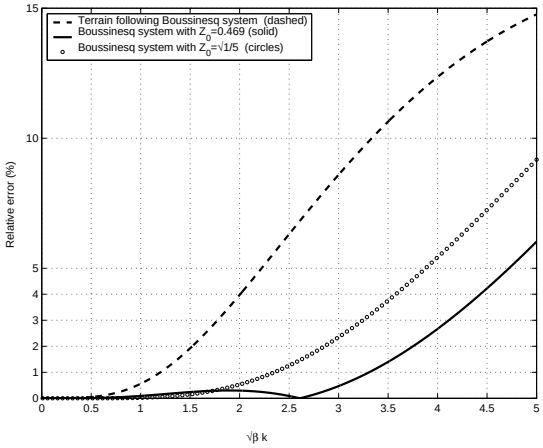

Fig. 4. Relative error of the phase velocity as a function of $\sqrt{\beta}k$ for the Boussinesq-type system (30)-(31) with $Z_0 = \sqrt{1/3}$ (the terrain-following system), $Z_0 = 0.469$ and $Z_0 = \sqrt{1/5}$.

parameter $\varepsilon \equiv a_o/\ell_p$ (a_o is the amplitude scale and ℓ_p is a wavelength scale). We start by using dimensionless parameters such as before. As pointed out in [10] the formulation naturally suggests combining these parameters as $\alpha\sqrt{\beta} \equiv \varepsilon$. Hence the characteristic depth h_o cancels out and the free surface perturbations are controlled through ε.

The novelty in the present formulation is that we can still accommodate the asymptotic modeling to consider very general topographic profiles, including multiply valued profiles as shown in [20]. As before we start from the nonlinear, dimensionless potential theory equations but follow an analytical route that is somewhat different from Matsuno's. Naturally some of the transforms used are similar, but they are "brought into the picture" by different means. In particular the Fourier analysis presented naturally suggests the use of FFT based methods to generate efficient numerical schemes.

We again use an orthogonal curvilinear coordinate system for the potential theory equations. Within this frame we are able to write a Dirichlet-to-Neumann (DtN) operator which automatically reduces the entire dynamics to the free surface. This formulation is possible in the presence of complex multi-valued profiles, or even rapidly varying topographies. Our transforms not only resemble, but are clearly related to, those in Matsuno [10] and in Byatt-Smith [36]. Some of the differences are that we work in Fourier space while Matsuno uses complex functions. In our formulation we work in the physical domain, through the curvilinear coordinate system and we arrive at Fourier-type transforms which are easily incorporated into a numerical method. The final result is a, variable coefficient, weakly nonlinear evolution equation of the Boussinesq-type. Our generalization of Matsuno's Boussinesq-type system has, as its (weakly dispersive) leading order approximation the terrain-following system presented in Nachbin [12]. This is a nice consistency check since here we do not use a power series expansion for the potential, but rather we do asymptotics with the Fourier operators.

Other very recent work include that of Craig and Sulem [37] which formulated an efficient spectral method based on the DtN operator. Their analysis differs from ours and Matsuno's but some resulting transforms are similar, in particular the Hilbert transform on a strip: namely equation (61) in the present paper, which appears as (18) in Matsuno [10] and as (27) in Craig and Sulem [37]). We recall that Matsuno's [10] as well as Craig and Sulem's analysis [37] are restricted to flat bottoms. In [38] Matsuno extended his analysis to mild slope bottom topographies, also using the conformal mapping strategy. Along these lines Zakharov *et al.* [39] using a Hamiltonian structure deduced exact (nonlinear) free surface equations in a fluid of infinite depth. The free surface is conformally mapped and Hilbert-differential equations are obtained along the free surface. The presence of Hilbert transforms has a clear connection with the three strategies mentioned above (including the present one). This is explicitly mentioned

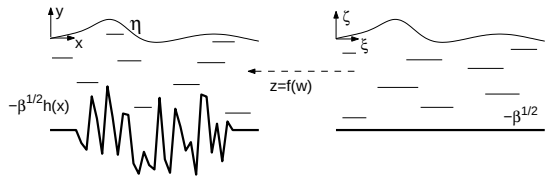

Fig. 5. Setup for the Schwarz-Christoffel transformation where $z = x + iy$ and $w = \xi + i\zeta$. The mapping is defined for the undisturbed configuration (i.e. with $\eta \equiv 0$).

by Zakharov *et al.* [39] in a reference to the work of Craig and Sulem [37]. In the presence of highly variable topographies we point out the very recent work by Keller [40]. A shallow water (hyperbolic) model is derived from the Euler equations by using curvilinear coordinates. This curvilinear coordinate system is based on smooth topographies or a smooth curve near the topography. We recall that in the present work our curvilinear coordinate system arises from a conformal transformation and therefore is valid for polygonal bottom profiles which need not be single-valued.

3.1 The inviscid and incompressible free boundary problem

As before, using the Schwarz-Christoffel transformation [24,25] we define a mapping from a uniform strip in the $\xi\zeta$-plane onto the undisturbed ($\eta \equiv 0$) corrugated strip in the physical xy-plane (c.f. figure 5). In the mapped domain we have $\zeta \equiv S(\xi, t) = \varepsilon N(\xi, t)$, while in the physical domain it is defined by $y(\xi, S(\xi, t)) = \alpha\eta(x(\xi, S(\xi, t)), t)$, with η denoting the surface gravity wave. When the free surface (FS) has a small steepness (as indicated by εN above) the Jacobian can be approximated as $|J| \approx y_\zeta^2(\xi, 0) + O(\varepsilon^2)$ [12].

As presented earlier the nonlinear potential theory equations in curvilinear $\xi\zeta$ coordinates, as presented in Nachbin [12] are

$$\phi_{\xi\xi} + \phi_{\zeta\zeta} = 0, -\sqrt{\beta} < \zeta < S(\xi, t). \tag{36}$$

where at the FS the free boundary conditions are

$$N_t + \frac{\alpha}{|J|}\phi_\xi N_\xi - \frac{1}{|J|\sqrt{\beta}}\phi_\zeta = 0 \tag{37}$$

$$\phi_t + \frac{\alpha}{2|J|}(\phi_\xi^2 + \phi_\zeta^2) + \eta = 0. \tag{38}$$

We have a trivial Neumann condition along the impermeable topography $\zeta \equiv -\sqrt{\beta}$: $\phi_\zeta = 0$. The scaling here corresponds to the third stage in the scaling sequence presented in figure 2. No approximation has been made up to this point.

3.2 The Dirichlet-to-Neumann (DtN) operator

In this subsection we briefly review Guidotti's time independent strategy [41] to formulate a DtN operator for a halfplane configuration as in figure 6. Then we will adapt this strategy to a time independent problem for a corrugated strip. Once this has been achieved we migrate this formulism to the nonlinear wave evolution problem and reduce the entire dynamics to the free surface.

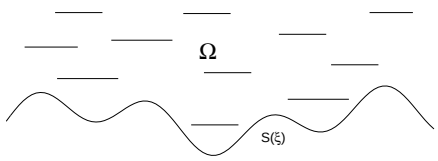

Fig. 6. Upper halfplane bounded by a corrugated curve $S(\xi)$.

3.2.1 The Dirichlet problem on a halfplane

Following [41], attention is given to periodic problems (say of period one) such that $\varphi(\xi),\ S(\xi) \in C_{per}([0,1])$. We have Laplace's equation in the domain Ω, above the curve $\Gamma \equiv (\xi, S(\xi))$, with Dirichlet data $\varphi(\xi)$ imposed along Γ. Let $(\xi, S(\xi))$ be a parametrization of the halfplane's (lower) boundary curve Γ. The mapping that takes the Dirichlet data onto its corresponding Neumann data we denote as

$$DtN[\varphi](\xi) = \partial_n \phi(\xi, S(\xi)), \tag{39}$$

where $\partial_n := \mathbf{n} \cdot (\partial_\xi, \partial_\zeta)$, $\mathbf{n} = |\Gamma_\xi|^{-1}(-S_\xi(\xi), 1)$ and $|\Gamma_\xi| = \sqrt{1 + S_\xi^2(\xi)}$.

As in classical potential theory, Guidotti suggests an integral representation for the potential

$$\phi(w) = \textstyle\int_\Gamma G(w - \tilde{w})\, f(\tilde{w}) d\Gamma,\ \tilde{w} \in \Gamma. \tag{40}$$

The unknown function f will be determined by the potential's Dirichlet data along Γ. By $d\Gamma$ we represent an infinitesimal boundary element and by $w = (\xi, \zeta)$ an interior point of our domain Ω. The 1-periodic version of the integral representation (40) is

$$\phi(\xi, \zeta) = \int_0^1 G(\xi - \tilde{\xi}, \zeta - S(\tilde{\xi}))\, f(\tilde{\xi}) |\Gamma_{\tilde{\xi}}| d\tilde{\xi}. \tag{41}$$

The periodic kernel proposed by Guidotti [41] has logarithmic singularities, in the form

$$G(\xi, \zeta) = \frac{1}{2\pi} \ln(1 + e^{-4\pi\zeta} - 2e^{-2\pi\zeta} \cos(2\pi\xi)), \tag{42}$$

and can also be represented by the Fourier series

$$G(\xi, \zeta) = -\sum_{\kappa \neq 0} \frac{1}{2\pi|\kappa|} e^{-2\pi|\kappa|\zeta} e^{2\pi i \kappa \xi} \qquad \text{if} \qquad \zeta \geq 0. \tag{43}$$

Hence the kernel is a harmonic function in the halfplane $\xi,\ \zeta > 0$, and 1-periodic in its first variable with the property that [41]

$$\lim_{\zeta \to 0^+} \partial_\zeta G(\xi, \zeta) = \lim_{\zeta \to 0^+} \frac{-2e^{-4\pi\zeta} + 2e^{-2\pi\zeta} \cos(2\pi\xi)}{1 + e^{-4\pi\zeta} - 2e^{-2\pi\zeta} \cos(2\pi\xi)} = \delta(\xi) - 1.$$

The Dirac delta is denoted by $\delta(\xi)$. Therefore one needs to be careful when deducing the DtN operator since an interior point will approach a boundary curve. This result is summarized in the following lemma proved in [41]:

Lemma: Let G be the Green's functions given above. Suppose that $S(\xi) \in C^1_{per}([0,1])$ represents a corrugated curve along the boundary of Ω. Then the following limit holds as an interior point approaches this boundary:

$$\lim_{w \to w_o} \int_\Gamma \partial_{n(w)} G(w - \tilde{w}) f(\tilde{w})\, d\Gamma_{\tilde{w}} = -f(w_o) + \fint_\Gamma \partial_{n(w_o)} G(w_o - \tilde{w}) f(\tilde{w})\, d\Gamma_{\tilde{w}}$$

$$\text{when} \qquad w \to w_o = (\xi_o, S(\xi_o)) \in \Gamma.$$

The limiting integral is given as a Cauchy Principal Value (indicated by a dash).

Clearly from the potential's integral representation (40) along the boundary we obtain

$$\varphi(w_o) = \int_{\Gamma} G(w_o - \tilde{w})\, f(\tilde{w}) d\Gamma_{\tilde{w}}, \tag{44}$$

where w_o is also along the boundary. Its periodic counterpart leads to the following Fredholm equation of the first kind in the source density f:

$$\varphi(\xi) = \int_0^1 G(\xi - \tilde{\xi}, \zeta - S(\tilde{\xi}))\, f(\tilde{\xi}) |\Gamma_{\tilde{\xi}}| d\tilde{\xi}. \tag{45}$$

Technical details on integral equations can be found in Taylor [42].

Once we find the singularity density $f(\xi)$ we use (40) (or its periodic counterpart (41)) and the lemma above to deduce an integral representation for the Dirichlet-to-Neumann operator

$$DtN(\varphi)(w_o) = \lim_{w \to w_o} \int_{\Gamma} \partial_{n(w)} G(w - \tilde{w}) f(\tilde{w})\, d\Gamma_{\tilde{w}},$$

where $w_o \in \Gamma$. In the periodic regime we have

$$DtN(\varphi)(\xi_o) = -f(\xi_o) + \int_0^1 \partial_{n(\xi_o)} G(\xi_o - \tilde{\xi}, S(\xi_o) - S(\tilde{\xi})) f(\tilde{\xi}) |\Gamma_{\tilde{\xi}}|\, d\tilde{\xi}. \tag{46}$$

Formally this completes the calculation of the DtN operator, assuming that at this stage the density f is known.

3.2.2 The Dirichlet problem on a corrugated strip

To simplify the presentation we first analyze the harmonic problem at a frozen instant of time:

$$\phi_{\xi\xi} + \phi_{\zeta\zeta} = 0 \quad \text{in} \quad -\sqrt{\beta} < \zeta < S(\xi) \tag{47}$$

$$\phi(\xi, S(\xi)) = \varphi(\xi) \quad \text{at the FS} \quad \zeta = S(\xi) \tag{48}$$

$$\phi_\zeta(\xi, -\sqrt{\beta}) = 0 \quad \text{at the topography} \quad \zeta = -\sqrt{\beta}. \tag{49}$$

By reflecting our domain about the topographic level curve $\zeta \equiv -\sqrt{\beta}$ we convert the mixed Dirichlet-Neumann problem above into a (pure) Dirichlet problem in the form

$$\phi_{\xi\xi} + \phi_{\zeta\zeta} = 0 \quad \text{in} \quad -2\sqrt{\beta} - S(\xi) < \zeta < S(\xi) \tag{50}$$

$$\phi = \varphi(\xi) \quad \text{at} \quad \zeta = S(\xi) \tag{51}$$

$$\phi = \varphi(\xi) \quad \text{at} \quad \zeta = -S(\xi) - 2\sqrt{\beta}. \tag{52}$$

Therefore the Neumann condition $\phi_\zeta(\xi, -\sqrt{\beta}) = 0$ is automatically satisfied. Again the time independent potential is cast into the integral representation

$$\phi(\xi, \zeta) = \int_0^1 K(\xi, \tilde{\xi}, \zeta, S(\tilde{\xi}))\, f(\tilde{\xi}) |\Gamma_{\tilde{\xi}}|\, d\tilde{\xi}, \tag{53}$$

where now the kernel has the form $K(\xi, \tilde{\xi}, \zeta, S(\tilde{\xi})) = G(s, -\zeta + \tilde{S}) + G(s, \zeta + \tilde{S} + 2\sqrt{\beta})$. We are basically using the Method of Images for the Green's function's logarithmic singularity. Our notation is such that $f(\tilde{\xi})$ is the symmetric source distribution over the top and bottom

boundary curves, $|\Gamma_\xi|^2 \equiv 1 + S_\xi^2(\xi)$, $s = \xi - \tilde{\xi}$ and $\tilde{S} = S(\tilde{\xi})$. Thus we have formally solved the potential problem (47)-(49) once we find the source distribution $f(\xi)$.

The integral representation in (53) can be written as

$$\phi(\xi,\zeta) = \int_0^1 K(\xi,\tilde{\xi},0,0)\; f(\tilde{\xi})|\Gamma_{\tilde{\xi}}|\, d\tilde{\xi} + \\ + \int_0^1 \{K(\xi,\tilde{\xi},\zeta,S(\tilde{\xi})) - K(\xi,\tilde{\xi},0,0)\}\; f(\tilde{\xi})|\Gamma_{\tilde{\xi}}|\, d\tilde{\xi}. \tag{54}$$

The first term, containing $K(\xi,\tilde{\xi},0,0)$, is the linear (singular) term corresponding to infinitesimal perturbations about the undisturbed water surface. In this way the nonlinear term arises as a *desingularized correction term*. Taking the normal derivative of the potential in (54) and letting the interior point approach the top boundary we obtain, in the limit, the Dirichlet-to-Neumann operator $DtN(\varphi)(\xi) \equiv \partial\phi/\partial n(\xi, S(\xi))$, which gives the Neumann data along the FS. Now we go back to calculating the source distribution $f(\xi)$ along the FS. Motivated by (54) we decompose the Dirichlet data into its linear and nonlinear parts: $\varphi(\xi) \equiv \varphi_L(\xi) + \varphi_{NL}(\xi)$.

The linear contribution

Using the Fourier representation of the Green's function G in the linear term of (54), and carefully computing the limit as we approach the top boundary, we have that $\varphi_L(\xi) = \mathbf{P}[f|\Gamma_\xi|\,]$ where

$$\mathbf{P}[f|\Gamma_\xi|\,] \equiv -\sum_{\kappa\neq 0} \frac{1 + e^{-2\pi|\kappa|2\sqrt{\beta}}}{2\pi|\kappa|}\; \mathbf{F}_\kappa[f|\Gamma_\xi|\,]e^{2\pi i\kappa\xi}. \tag{55}$$

By $\mathbf{F}_\kappa[g]$ we denote the k-th Fourier coefficient of the one-periodic function $g(\xi)$. The contribution from the linear part is easily computed through $f|\Gamma_\xi| = \mathbf{P}^{-1}[\varphi_L]$. This is equivalent to the (linear) flat FS case, but recall that for weakly nonlinear waves $S(\xi) = O(\varepsilon)$. Hence we will seek an $O(\varepsilon)$ approximation of $f(\xi)$ from the full representation (54).

The nonlinear contribution

The integral equation (54), evaluated along the boundary curve $\zeta = S(\xi)$, can be written in a more compact (operator) notation

$$\varphi(\xi) = \mathbf{P}[f|\Gamma_\xi|\,] + \mathbf{Q}_S[f|\Gamma_\xi|\,]. \tag{56}$$

The nonlinear (S-dependent) contribution is identified by the operator $\mathbf{Q}_S[\cdot]$. The main difficulty resides on inverting (54) and computing the source distribution $f(\xi)$ along the nonlinear FS, in the presence of a kernel depending on S. As presented in detail in [20], we can characterize the leading order approximation $\mathbf{R}_S$ to the fully nonlinear operator $\mathbf{Q}_S$. Namely we have that

$$\mathbf{R}_S[f|\Gamma_\xi|\,] = S\sum_{\kappa\neq 0}\{-1 + e^{-2\pi|\kappa|2\sqrt{\beta}}\}\mathbf{F}_\kappa[f|\Gamma_\xi|\,]e^{2\pi i\kappa\xi} + \\ + \sum_{\kappa\neq 0}\{1 + e^{-2\pi|\kappa|2\sqrt{\beta}}\}\mathbf{F}_\kappa[Sf|\Gamma_\xi|\,]e^{2\pi i\kappa\xi}.$$

After some algebra we obtain a weakly nonlinear approximation, for the inversion procedure, leading to a source distribution

$$f(\xi)|\Gamma_\xi| = \mathbf{P}^{-1}[\varphi] - \mathbf{P}^{-1}[S\,DtN_0[\varphi]\,] + \sum_{\kappa\neq 0} 2\pi|\kappa|\mathbf{F}_\kappa[S\,\mathbf{P}^{-1}[\varphi]\;]e^{2\pi i\kappa\xi} + O(\varepsilon^2). \tag{57}$$

The nice thing about this approximation for source distribution $f(\xi)$ is that it is expressed by a linear contribution (inverting (55)) composed with ($S(\xi)$-dependent) iterates of linear objects: namely the linear ($S \equiv 0$) Dirichlet-to-Neumann operator DtN_0 and again $\mathbf{P}^{-1}[\varphi]$. In the sequel we will confirm this interpretation for the DtN_0 operator. Thus we have approximated the calculation of the source distribution by straightforward Fourier transforms (namely FFTs) of smooth functions. We will now show how the nonlinear DtN operator can be approximated by straightforward compositions of the linear DtN_0 operator. This is achieved by using the approximation given in (57).

3.3 Evolution equations for weakly nonlinear surface gravity waves

In the context of nonlinear surface gravity waves, the Neumann data is needed at the second FS condition. Writing the norm (squared) of the velocity in terms of its tangential and normal components, implies that we need to find the ξ and ζ derivatives as in

$$DtN[\varphi](\xi) \equiv \partial_n \phi(\xi, S) = \left[-\frac{S_\xi}{|\Gamma_\xi|}\phi_\xi + \frac{1}{|\Gamma_\xi|}\phi_\zeta \right]_{(\xi,S)}. \tag{58}$$

First we differentiate (54) with respect to ζ and use (57) having $\zeta = S$. After a lengthy calculation we obtain the compact expression

$$\phi_\zeta = DtN_0[\varphi - S\, DtN_0[\varphi]\,] - S\varphi_{\xi\xi} + O(\varepsilon^2). \tag{59}$$

When $S \equiv 0$, ζ is the normal direction and (59) is exact, confirming the interpretation given to DtN_0. There are other useful ways of representing the $DtN_0[\varphi] \equiv \mathbf{T}[\varphi_\xi]$:

$$\mathbf{T}[\varphi_\xi] = -i \sum_{\kappa \neq 0} \tanh[2\pi\kappa\sqrt{\beta}]\mathbf{F}_\kappa[\varphi_\xi] e^{2\pi i \kappa \xi}. \tag{60}$$

Note that the dispersion relation appears as the symbol of the linear DtN_0 operator. For example in Berger and Milewski [43] a Fourier-type integral transform, also having the dispersion relation as its symbol, is used in studying surface gravity wave interaction and wave-turbulence. This also appears in the work by Craig and Sulem [37]. As mentioned earlier, we point out that $\mathbf{T}$ is the periodic counterpart of the (singular) integral operator used by Matsuno [10] and also referred to in Craig and Sulem [37] as the *Hilbert transform on the strip*:

$$\tilde{\mathbf{T}}[\varphi_x] = \frac{1}{2\sqrt{\beta}} \int_{-\infty}^{\infty} \frac{\varphi_x(x')}{\sinh[\frac{\pi}{2\sqrt{\beta}}(x - x')]} dx'. \tag{61}$$

Recalling that the surface wave profile is denoted by $S(\xi, t) \equiv \varepsilon N(\xi, t)$ we put together equations (58) and (59), and use the operator $\mathbf{T}$, to write (omitting some steps; c.f. [20]) the set of reduced equations

$$\eta_t - \frac{1}{M\sqrt{\beta}} \big\{ \mathbf{T}[U] + \varepsilon \big((\frac{\eta U}{M})_\xi + \mathbf{T}[\frac{\eta}{M}\, \mathbf{T}[U]_\xi] \big) \big\} = O(\varepsilon^2). \tag{62}$$

$$U_t + \eta_\xi + \varepsilon \left(\frac{1}{2\sqrt{\beta}} \Big((\frac{U^2}{M^2})_\xi + (\frac{1}{2M^2})_\xi \mathbf{T}[U]^2 \Big) - (\frac{\eta}{M})_\xi \mathbf{T}[\eta_\xi] \right) = O(\varepsilon^2). \tag{63}$$

where we have that $\phi_\xi \equiv U$. Dropping the $O(\varepsilon^2)$ terms in equations (62) and (63) we get a *fully dispersive terrain-following Boussinesq system*. For a flat bottom (i.e. $M(\xi) \equiv 1$) this system reduces to system (19)-(20) in Matsuno [10]. Also by expanding in β, for the weakly dispersive regime, we can recover the terrain-following Boussinesq system as in [12], when using the vertically averaged terrain-following velocity component (equation (5.12) in [12]).

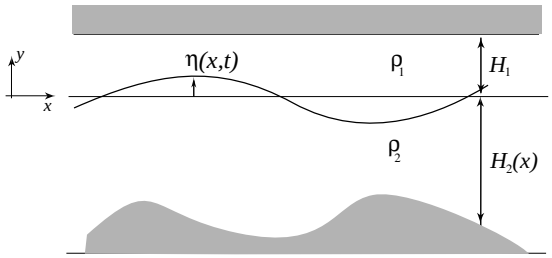

Fig. 7. Internal wave in a two-layer system.

4 Internal waves

For oceanic applications, we consider a two-layer system with a small density jump and assume that the top free surface affects little on the motion of the interface between the two layers and can be replaced by a rigid wall. Here, we therefore introduce mathematical models describing the internal wave (baroclinic) mode only, but the extension to the case when the surface wave (barotropic) mode is non-negligible is straight-forward [44].

In a two-layer system of two different densities of ρ_1 and ρ_2 (assuming $\rho_1 < \rho_2$ for a stable stratification), the governing equation in each layer is the Laplace equation for the velocity potential $\tilde{\phi}_i$ $(i = 1, 2)$:

$$\tilde{\phi}_{1\tilde{x}\tilde{x}} + \tilde{\phi}_{1\tilde{y}\tilde{y}} = 0 \quad \text{for} \quad \tilde{\eta}(\tilde{x}, \tilde{t}) < \tilde{y} < \tilde{H}_1, \quad -\infty < \tilde{x} < \infty, \tag{64}$$

$$\tilde{\phi}_{2\tilde{x}\tilde{x}} + \tilde{\phi}_{2\tilde{y}\tilde{y}} = 0 \quad \text{for} \quad -\tilde{H}_2(\tilde{x}) < \tilde{y} < \tilde{\eta}(\tilde{x}, \tilde{t}), \quad -\infty < \tilde{x} < \infty, \tag{65}$$

where $i = 1$ ($i = 2$) represents the upper (lower) layer, $\tilde{\eta}$ is the displacement of the interface between the two layers, and $\tilde{H}_i$ is the layer thickness. The boundary conditions at the interface are the continuity of normal velocity and pressure across the interface:

$$\tilde{\eta}_t + \tilde{\phi}_{i\tilde{x}}\tilde{\eta}_{\tilde{x}} = \tilde{\phi}_{i\tilde{y}}, \quad \text{at} \quad \tilde{y} = \tilde{\eta}(\tilde{x}, t), \tag{66}$$

$$\tilde{p}_1 = \tilde{p}_2 \qquad \text{at} \quad \tilde{y} = \tilde{\eta}(\tilde{x}, t), \tag{67}$$

where the pressure $\tilde{p}_i$ can be found from the Bernoulli equation:

$$\tilde{\phi}_{i\tilde{t}} + \frac{1}{2}\left(\tilde{\phi}_{i\tilde{x}}^{\,2} + \tilde{\phi}_{i\tilde{y}}^{\,2}\right) + g\tilde{\eta} + \frac{\tilde{p}_i}{\rho_i} = 0. \tag{68}$$

The boundary conditions at the flat top and at the variable bottom are given by

$$\tilde{\phi}_{1\tilde{y}} = 0 \quad \text{at } \tilde{y} = \tilde{H}_1, \qquad \tilde{\phi}_{2\tilde{y}} + \tilde{H}_{2\tilde{x}}\tilde{\phi}_{2\tilde{y}} = 0 \quad \text{at } \tilde{y} = -\tilde{H}_2(\tilde{x}). \tag{69}$$

When these basic equations are non-dimensionalized in a similar way to surface wave problems discussed in the preceding sections, in addition to the two dimensionless parameters (α and β) introduced to measure nonlinear and dispersive effects, respectively, there is another independent parameter: the depth ratio defined by H_2/H_1. The behaviors of the linear dispersion relation for long waves vary depending on this depth ratio and, therefore, different asymptotic regimes are possible. In the absence of bottom topography (H_2=constant), with linearizing the free surface boundary conditions given by (66)–(67), the dispersion relation between wave speed C and wave number k [45] can be found as

$$C^2 = \frac{(g/k)(\rho_2 - \rho_1)}{\rho_1 \coth kH_1 + \rho_2 \coth kH_2}\,. \tag{70}$$

Under the long wave assumption (for definiteness, $(kH_1)^2 = O(\beta) \to 0$), depending on the depth ratio or, equivalently, kH_2, we have the following three regimes of interest:

(i) as $kH_i \to 0$ (shallow water),

$$C = C_0 \left[1 - \frac{k^2}{6}\frac{\rho_1 {H_1}^2 H_2 + \rho_2 H_1 {H_2}^2}{\rho_1 H_2 + \rho_2 H_1} + O(k^4 H_i^4)\right], \quad {C_0}^2 = \frac{gH_1H_2(\rho_2 - \rho_1)}{\rho_1 H_2 + \rho_2 H_1}, \tag{71}$$

(ii) as $kH_1 \to 0$ and $kH_2 = O(1)$ (deep water),

$$C = C_0 \left[1 - \frac{1}{2}\left(\frac{\rho_2}{\rho_1}\right) kH_1 \coth kH_2 + O(k^2 {H_1}^2)\right], \quad {C_0}^2 = gH_1\left(\frac{\rho_2}{\rho_1} - 1\right), \tag{72}$$

(iii) as $kH_1 \to 0$ and $kH_2 \to \infty$ (infinitely deep water),

$$C = C_0 \left[1 - \frac{1}{2}\left(\frac{\rho_2}{\rho_1}\right) |k| H_1 + O(k^2 {H_1}^2)\right], \quad {C_0}^2 = gH_1\left(\frac{\rho_2}{\rho_1} - 1\right). \tag{73}$$

Since the leading-order dispersive effects appear at $O(\beta)$ for shallow water and $O(\beta^{1/2})$ for deep or infinitely deep water, the balance between nonlinearity and dispersion can occur in different orders of approximation. For shallow water, the appropriate scaling between α and β is $\alpha = O(\beta)$, while $\alpha = O(\beta^{1/2})$ for deep or infinitely deep water. For weakly nonlinear unidirectional waves, these different scalings lead to different mathematical models: the Korteweg-deVries (KdV) equation [46], the Intermediate Long Wave (ILW) equation [47,48], and the Benjamin-Ono (BO) equation [49,50] in the shallow, deep, and infinitely deep water regimes, respectively. For arbitrary depth ratio, more general forms of weakly nonlinear model equations have been derived by Matsuno [51] and Choi and Camassa [44].

Despite their substantial simplification of the original problem, the weakly nonlinear internal wave models have been found to be inadequate for large amplitude internal waves commonly observed in recent field experiments. To capture finite amplitude effects accurately, under the sole assumption that the waves are long compared with the thickness of one layer, strongly nonlinear models have been derived by Choi and Camassa [52,53] for both shallow and deep water configurations. In their derivation, $\beta \ll 1$ has been assumed, but no assumption on wave amplitude has been made so that $\alpha = O(1)$.

4.1 The strongly nonlinear model for the shallow configuration

For the shallow configuration, we assume that $H_2/H_1 = O(1)$ along with $H_1/l_p \ll 1$ and non-dimensionalize all physical variables as

$$\tilde{x} = l_p x, \quad \tilde{y} = H_1 y, \quad \tilde{t} = \left(\frac{l_p}{c_0}\right) t, \quad \tilde{\eta} = H_1 \eta, \quad \tilde{\phi_i} = \left(\frac{g l_p H_1}{c_0}\right) \phi_i, \quad \tilde{p_i} = \rho_1 {c_0}^2 p_i, \tag{74}$$

where l_p is the typical horizontal wavelength and ${c_0}^2 = gH_1$. Notice that, for strongly nonlinear waves, we scale the interface displacement $\tilde{\eta}$ by H_1, instead of wave amplitude a that is commonly used for a weakly nonlinear analysis. As a result, α no longer appears in dimensionless equations and β is the only small parameter in the problem. Then, after the velocity potentials are expanded as

$$\phi_1 = \sum_{n=0}^{\infty} \frac{(-\beta)^n}{(2n)!}(y - H_1)^{2n} \frac{\partial^{2n} f_1}{\partial x^{2n}}, \quad \phi_2 = \sum_{n=0}^{\infty} \frac{(-\beta)^n}{(2n)!}(y + H_2)^{2n} \frac{\partial^{2n} f_2}{\partial x^{2n}}, \tag{75}$$

the kinematic and dynamic free surface boundary conditions given by (66)–(67) with (68) form a system of four equations for η, f_1, f_2, and the pressure at the interface $P(x,t) \equiv p(x, y = \eta, t)$. Introducing the depth averaged velocity U_i and neglecting terms of $O(\beta^2)$ lead to a system of nonlinear evolution equations [52]:

$$h_{it} + (h_i U_i)_x = 0, \tag{76}$$

$$U_{it} + U_i U_{ix} + \eta_x = -\frac{\rho_1}{\rho_i} P_x + \frac{\beta}{h_i}\left(\frac{1}{3} {h_i}^3 G_i\right)_x + O(\beta^2)\,, \tag{77}$$

where the layer thickness h_i and the depth-averaged velocity U_i are defined by

$$h_1(x,t) = H_1 - \eta(x,t)\ , \quad U_1(x,t) = \frac{1}{h_1}\int_{\eta}^{H_1} \phi_{1x}(x,y,t)\,\mathrm{d}y\,, \tag{78}$$

$$h_2(x,t) = H_2(x) + \eta(x,t), \qquad U_2(x,t) = \frac{1}{h_2}\int_{-H_2(x)}^{\eta} \phi_{2x}(x,y,t)\,\mathrm{d}y\,. \tag{79}$$

Unlike the weakly nonlinear case, it can be seen that the strongly nonlinear model contains the nonlinear dispersive effect denoted by G_i:

$$G_i(x,t) = U_{ixt} + U_i U_{ixx} - (U_{ix})^2\,, \tag{80}$$

which comes from a non-hydrostatic pressure contribution with an error of $O(\beta^2)$. Alternatively, the same system can be derived from the Euler equations without introducing the velocity potential [52] or from physical conservation laws of mass, momentum, and energy [54].

As demonstrated in Choi and Camassa [52] and Camassa *et al.* [55], solitary wave solutions of the strongly nonlinear model show excellent agreement with numerical solutions of the Euler equations as well as laboratory experiments even when the wave amplitude is close to a maximum value given by $a_m = (H_1 - H_2\sqrt{\rho_1/\rho_2})/(1+\sqrt{\rho_1/\rho_2})$ for which the solitary wave becomes a front. This is a unique feature of internal waves and energy-conserving front solutions are impossible for surface waves.

It is interesting to notice that, for the single layer ($\rho_1 = 0$) case, the system given by (76)–(77) for the lower layer ($i = 2$) can be reduced to that of Su and Gardner [56] (which is also called the Green-Naghdi equations [57] in the literature). As shown in Li *et al.* [58], in terms of solitary wave interactions, this strongly nonlinear system for surface waves compares better with the Euler equations than the weakly nonlinear model up to intermediate wave amplitudes, beyond which the local wave steepness increases with wave amplitude and the long wave assumption becomes invalid. On the other hand, for internal solitary waves, the characteristic wavelength increases with wave amplitude and the long wave assumption becomes more relevant for the large-amplitude regimes. This explains why the strongly nonlinear internal wave model is so successful when compared with laboratory and field observations.

When solving the time-dependent equations numerically, care must be taken since the system might suffer from the Kelvin-Helmholtz instability caused by a horizontal velocity jump [59] and short wave perturbations could grow exponentially fast. Keeping in mind that the system is derived under the inviscid fluid assumption where no tangential velocity continuity is required, such instability is expected unless short wave disturbances are effectively filtered out. A numerical regularization technique must be applied to solve the system of time-dependent equations given by (76)–(77). Notice that this instability is not an outcome of asymptotic expansion but that of inviscid assumption; therefore, it is still unavoidable even when solving the full Euler equations [60].

In presence of slowly varying bottom topography with $\gamma = O(1)$, the strongly nonlinear model is further generalized to include the effect of bottom topography by adding the following term to the right-hand side of (77) for the lower layer [59]:

$$B_2 = -\frac{\beta}{\eta_2}\left[\frac{{\eta_2}^2}{2}\left(\frac{\partial}{\partial t} + U_2\frac{\partial}{\partial x}\right)(U_2 H_{2x})\right]_x + \beta\left[\frac{\eta_2}{2}G_2 - \left(\frac{\partial}{\partial t} + U_2\frac{\partial}{\partial x}\right)(U_2 H_{2x})\right] H_{2x}\,. \tag{81}$$

For rapidly varying bottom topography with $\gamma \ll 1$, the same method described in section 2 can be used for the lower layer and the evolution equations for the lower layer written in curvilinear coordinates are expected to be coupled with those for the upper layer through the pressure continuity condition.

4.2 The strongly nonlinear model for the deep configuration

In deep configuration, we assume that $H_1/l_p \ll 1$ and $H_2/l_p = O(1)$ which, from the continuity equation, results in the following scalings

$$\tilde{w}_1/\tilde{u}_1 = O(H_1/l_p) = O(\beta^{1/2})\,, \qquad \tilde{w}_2/\tilde{u}_2 = O(H_2/l_p) = O(1)\,, \tag{82}$$

and, from continuity of normal velocity at $y = \tilde{\eta}$,

$$\tilde{w}_2/\tilde{u}_1 = O(\beta^{1/2})\,, \qquad \tilde{u}_2/\tilde{u}_1 = O(\beta^{1/2}) \qquad \text{at} \quad \tilde{y} = \tilde{\eta}\,, \tag{83}$$

where u_i and w_i are the horizontal and vertical velocities, respectively. These scalings imply that the upper layer is more active than the lower layer and nonlinear effects become more important in the shallow upper layer. Therefore, the evolution equations for the upper layer can be obtained from the leading order approximation to (76)–(77) as

$$\eta_t - \Big[(1-\eta)U_1\Big]_x = 0\,, \tag{84}$$

$$U_{1t} + U_1 U_{1x} + \eta_x = -P_x + O(\beta)\,. \tag{85}$$

An expression for the pressure at the interface P can be found by solving the linear potential theory problem for the lower layer [52] to give

$$\eta_t - \Big[(1-\eta)U_1\Big]_x = 0\,, \tag{86}$$

$$U_{1t} + U_1 U_{1x} + (\rho_2/\rho_1 - 1)\,\eta_x = \beta^{1/2}(\rho_2/\rho_1)\mathcal{T}\Big[(h_1 - \zeta)\bar{u}_1\Big]_{xt}\,, \tag{87}$$

where the nonlocal operator $\mathcal{T}$ is defined as

$$\mathcal{T}[f] = \frac{1}{2H_2}\fint_{-\infty}^{\infty} f(x')\,\coth\left[\frac{\pi}{2H_2}(x'-x)\right]\,\mathrm{d}x'\,. \tag{88}$$

As $H_2 \to \infty$, the operator $\mathcal{T}$ becomes the Hilbert transform in the lower half plane. Once again, solitary wave solutions of the strongly nonlinear model for the deep configuration are found to compare well with laboratory experiments [52,55].

References

1. R. Burridge, G. Papanicolaou, and B. White, SIAM J. Appl. Math. **47** (1987) pp. 146-168.
2. C.C. Mei, *The Applied Dynamics of Ocean Surface Waves*, (John Wiley 1983).
3. P.G. Baines, *Topographic Effects in Stratified Flows*, (Cambridge Univ. Press, 1995).
4. European Centre for Medium-Range Weather Forecasts (ECMWF), *Orography*, (1998).
5. D.H. Peregrine, J. Fluid Mech. **27** (1967), pp. 815-827.
6. A.B. Kennedy, J.T. Kirby, Q. Chen and R.A. Dalrymple, Wave Motion **33** (2001) pp. 225-243.
7. P.A. Madsen, R. Murray and O.R. Sørensen, Coastal Engineering **15** (1991), pp. 371-388.
8. P.A. Madsen and O.R. Sørensen, Coastal Engineering **18** (1992), pp. 183-205.
9. O. Nwogu, Coastal and Ocean Engineering **119** (1993), pp. 618-638.
10. Y. Matsuno, Phys. Rev. Lett. **69** (1992), 609.
11. H.A. Schäffer and P.A. Madsen, Coastal Engineering **26** (1995), pp. 1-14.
12. A. Nachbin, SIAM Appl. Math. **63** (2003), pp. 905-922.
13. J.C. Muñoz Grajales and A. Nachbin, SIAM J. Appl. Math. **64**, (2004) pp. 977-1001.
14. J.C. Muñoz Grajales and A. Nachbin, SIAM Multiscale Model. Simul. **3**, (2005) pp. 680-705.
15. J.P. Fouque, J. Garnier and A. Nachbin, SIAM J. Appl. Math. **64**, (2004) pp. 1810-1838.
16. J.P. Fouque, J. Garnier, J.C. Muñoz, and A. Nachbin, Phys. Rev. Lett. **92** (2004), 094502-1.
17. J.R. Quintero and J.C. Muñoz Grajales, Meth. Appl. Anal. **11** (2004), pp. 15-32.
18. J.C. Muñoz Grajales and A. Nachbin, IMA J. Appl. Math. **71** (2006) pp. 600-633.

19. W. Artiles and A. Nachbin, Phys. Rev. Lett. **93** (2004), 234501.
20. W. Artiles and A. Nachbin, Meth. Appl. Anal. **11** (2004), pp. 1-18.
21. C. Pires and M.A. Miranda, J. Geophys. Res. **106** (2001), pp. 19733–19796.
22. G.B. Whitham, *Linear and nonlinear waves*, (John Wiley, 1974).
23. R.R. Rosales and G.C. Papanicolaou, Studies in Appl. Math. **68** (1983), pp. 89–102.
24. T. Driscoll, http://www.math.udel.edu/driscoll/software.
25. T. Driscoll and L.N. Trefethen, *Schwarz-Christoffel Mapping*, (Cambridge Univ. Press, 2002).
26. M. Asch, W. Kohler, G. Papanicolaou, M. Postel and B. White, SIAM Review **33**, (1991) pp. 519-625.
27. J.P. Fouque, and A. Nachbin, SIAM Multiscale Model. Simul. **1**, (2003), pp. 609-629.
28. J.P. Fouque, J. Garnier, and A. Nachbin, Physica D **195** (2004), pp. 324-346.
29. J.P. Fouque, J. Garnier, G.C. Papanicolaou and K. Sølna, *Wave Propagation and Time Reversal in Randomly Layered Media*, (Springer-Verlag, to appear 2007).
30. J. Garnier and A. Nachbin, Phys. Rev. Lett. **93** (2004), 154501.
31. A. Nachbin, *Modelling of Water Waves in Shallow Channels*, (Computational Mechanics Publications, Southampton, U.K., 1993).
32. A. Nachbin, J. Fluid Mech. **296** (1995), pp. 353-372.
33. A. Nachbin and G.C. Papanicolaou, J. Fluid Mech. **241** (1992), pp. 311–332.
34. Yoon, S.B. and Liu, P.L.F. J. Fluid Mech. **205** (1989) pp. 397-419.
35. J. Hamilton, J. Fluid Mech. **83** (1977), pp. 289-310.
36. J.G.B. Byatt-Smith, J. Fluid Mech. **49** (1971), pp. 625-633.
37. W. Craig and C. Sulem, J. Comput. Phys. **108** (1993), pp. 73-83.
38. Y. Matsuno, J. Fluid Mech. **249** (1993) pp. 121-133.
39. V.E. Zakharov, A.I. Dyachenko and O.A. Vasilyev, Euro. J. Mech. B/Fluids **21** (2002), pp. 283-291.
40. J.B. Keller, J. Fluid Mech. **489** (2003), pp.345-348.
41. P. Guidotti, J. Comput. Phy. **190** (2003), pp. 325-345.
42. M.E. Taylor, *Partial Differential Equations I: Basic Theory*, (Springer Verlag, 1996).
43. K.M. Berger and P.A. Milewski, SIAM J. Appl. Math. **63** (2003), pp. 1121-1140.
44. W. Choi and R. Camassa, J. Fluid Mech. **313** (1996), pp. 83–103.
45. H. Lamb, *Hydrodynamics,* (Dover, 1932.)
46. T. B. Benjamin, J. Fluid Mech. **25** (1966), pp. 241–270.
47. R. I. Joseph, J. Phys. A: Math. Gen. **10** (1977), L225–L227.
48. K. Tung, T. F. Chan and T. Kubota, Stud. Appl. Maths **66** (1982), pp. 1–44.
49. T. B. Benjamin, J. Fluid Mech. **29** (1967), pp. 559–592.
50. H. Ono, J. Phys. Soc. Japan **39** (1975), 1082–1091.
51. Y. Matsuno, J. Phys. Soc. Japan **62** (1993), 1902–1916.
52. W. Choi and R. Camassa, J. Fluid Mech. **396**, 1–36.
53. W. Choi and R. Camassa, Phys. Rev. Lett. **77** (1996), 1759–1762.
54. M. Miyata, Proc. IUTAM Symp. on Nonlinear Water Waves, Horikawa, H. and Maruo, H. (eds), 399 (1988).
55. R. Camassa, W. Choi, H. Michallet, P.-O. Rusås and J. K. Sveen, J. Fluid Mech., **549** (2006), pp. 1–23.
56. C. H. Su and C. S. Gardner, J. Math. Phys. **10** (1969), pp. 536–539.
57. A. E. Green and P. M. Naghdi, J. Fluid Mech. **78** (1976), pp. 237–246.
58. Y. A. Li, J. M. Hyman and W. Choi, Stud. Appl. Math. **113** (2004), pp. 303–324.
59. T. Jo and W. Choi, Stud. Appl. Math. **109** (2002), pp. 205–228.
60. J. Grue, H. A. Friis, E. Palm and P. O. Rusas, J. Fluid Mech. **351** (1997) pp. 223–252.